ACCOUNTS of chemical research

pubs.acs.org/accounts Article

Tuning Interfacial Chemistry to Direct the Electrosynthesis of Metal Oxide Semiconductors

Published as part of the Accounts of Chemical Research special issue "Electrosynthesis of Inorganic Materials".

Krishnan Rajeshwar,* Abbas Vali, Abhishek Rawat, and Noseung Myung

Cite This: *Acc. Chem. Res.* 2023, 56, 994−1003 Read Online

ACCESS | Metrics & More | Article Recommendations

CONSPECTUS: Metal oxide semiconductors have many features that make them attractive for both fundamental and applied studies. For example, these compounds contain elements (e.g., Fe, Cu, Ti, etc.) that are derived from minerals rendering them earth-abundant and, most often, are also not toxic. Therefore, they have been examined for possible applicability in a very diverse range of technological applications including photovoltaic solar cells, charge storage devices, displays, smart windows, touch screens, etc. The fact that metal oxide semiconductors have both *n*- and *p*-type conductivity makes them amenable for use as hetero- or homojunctions in microelectronic devices and as photoelectrodes in solar water-splitting devices. This Account presents a review of collaborative research on the electrosynthesis of metal oxides from our respective groups against the backdrop of key developments on this topic. The many variants that interfacial chemical modification schemes offer are shown herein to lead to the targeted synthesis of a wide array of not only simple binary metal oxides but also more complex chemistries involving multinary compound semiconductors and alloys.

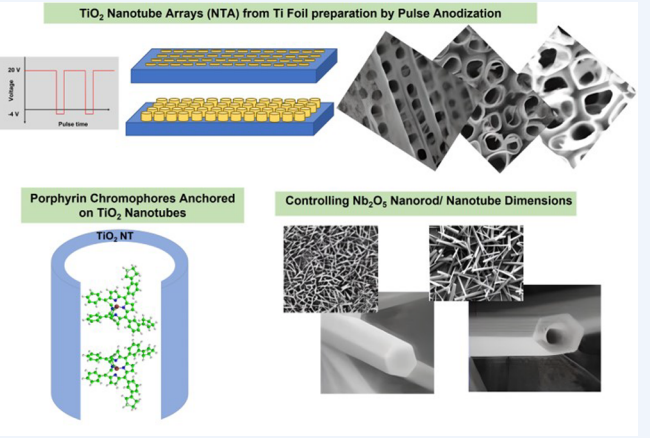

This Account presents our perspective on how parallel developments in the understanding of and ability to manipulate electrode−electrolyte interfaces have correspondingly enabled the innovation of a broad array of electrosynthetic strategies. These coupled with the advent of versatile tools to probe interfacial processes (undoubtedly, a child of the nanotechnology "revolution") afford an operando examination of how effective the strategies are to secure the targeted metal oxide product as well as the mechanistic nuances. Flow electrosynthesis, for example, removes many of the complications accruing from the accumulation of interfering side products—veritably, this is an Achilles heel of the electrosynthesis approach. Coupling flow electrosynthesis with downstream analysis tools based on spectroscopic or electroanalytical probes opens up the possibility of immediate process feedback and optimization. The combination of electrosynthesis, stripping voltammetry, and electrochemical quartz crystal nanogravimetry (EQCN), either in a static or in a dynamic (flow) platform, is shown below to offer intriguing possibilities for metal oxide electrosynthesis. While many of the examples below are based on our current and recent research and in other laboratories, unlocking even more potential will hinge on future refinements and innovations that surely are around the corner.

KEY REFERENCES

- Schlesinger, T. E.; Rajeshwar, K.; de Tacconi, N. R. Electrodeposition of Semiconductors. In *Modern Electroplating*; Schlesinger, M., Ed.; Springer: New York, 2010; Chapter 14, pp 383−411.[1] *While metal chalcogenides perhaps have dominated the field of semiconductor electrosynthesis, the burgeoning literature on the electrosynthesis of metal oxide semiconductors (up to ∼2010) is reviewed here.*
- Yamamoto, J.; Tan, A.; Shiratsuchi, R.; Hayase, S.; Chenthamarakshan, C. R.; Rajeshwar, K. A 4% Dye-Sensitized Solar Cell Fabricated from Cathodically Electrosynthesized Composite Titania Films. *Adv. Mater.* **2003**, *15*, 1823−1825.[2] *This early study demonstrated that electrosynthesis indeed could furnish high-performing metal oxide semiconductors in a solar cell application.*

Received: December 22, 2022
Published: April 19, 2023

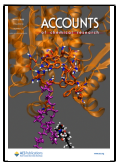

Table 1. Binary Oxide Semiconductors That Have Been Electrosynthesized

semiconductor	band gap (eV)[a]	electrosynthesis type	comments	ref[b]
ZnO	3.37	cathodic	base electrogeneration	1, 7
		cathodic	use of an oxygenated nonaqueous bath (e.g., DMSO)	1
WO_3	3.0−3.3	cathodic	uses tungsten powder in hydrogen peroxide bath	1, 7
		anodic	anodization of W foil in corrosive media also containing other (e.g., organic) additives	1, 7
TiO_2	3.0−3.2	cathodic	the titanyl ion is generated followed by pH control and thermal anneal	1, 7
		anodic	Ti(III) species in acidic aqueous $TiCl_3$ bath oxidized to Ti(IV) precursor gel followed by thermal anneal	8
		anodic	anodization (like one above for WO_3) results in self-assembled nanotubular arrays (NTAs)	1, 7
SnO_2	3.6	cathodic	base electrogeneration	1, 7
CdO	2.2	cathodic	base electrogeneration use of an oxygenated nonaqueous bath (e.g., DMSO)	1
		cathodic		1
Fe_2O_3	2.2	anodic	oxidation of Fe(II) species to Fe(III) followed by thermal anneal	7
		cathodic	a base electrogeneration variant using H_2O_2 reduction	9
		cathodic	use of a mixed ethanol−water bath	10
Bi_2O_3	2.3−3.3	two-step	cathodic deposition of metal film followed by anodic stripping in a precipitating medium (see text)	3
Cu_xO	1.2−2.2	cathodic	perhaps the most widely studied	1, 7

[a]The values listed here are approximate and should serve only as a guide. They hinge on whether the optical transition is direct or indirect and on a variety of other factors; some are intrinsic to the materials, and the others are measurement or analysis related. This also reflects the varying precision with which the values are quoted. See also ref 11 for a fuller discussion. [b]Review articles rather than the original works are cited here for the most part because these also contain discussions on related studies; the exceptions are refs 8−10.

Table 2. Some Ternary Oxide Semiconductors That Have Been Electrosynthesized

semiconductor	band gap (eV)[a]	electrosynthesis type	comments	ref
$CuWO_4$	2.0−2.3	cathodic	base electrogeneration using *p*-benzoquinone followed by thermal anneal	7
BiOI	1.85	cathodic	base electrogeneration variant using bismuth nitrate in a KI complexing medium	7
$BiVO_4$	2.4	two-step	see above example in Table 1 for bismuth oxide	3
Ag_3VO_4	2.1−2.6	two-step	a nonaqueous medium is used for first (metal deposition) step	12
$AgVO_3$	1.94−2.72	two-step	pH used as a tool to select the vanadium species for precipitation	13

[a]The values listed here are approximate and should serve only as a guide. They hinge on whether the optical transition is direct or indirect and on a variety of other factors; some are intrinsic to the materials, and the others are measurement or analysis related. This also reflects the varying precision with which the values are quoted. See also ref 11 for a fuller discussion.

Table 3. Examples of Hybrid Syntheses of Ternary MO Semiconductors

ternary oxide	electrosynthesis step	nonelectrochemical step	ref
$BiVO_4$	cathodic deposition of Bi metal from an ethylene glycol bath	conversion to product after soaking in $VO(acac)_2$ and thermolysis in air at 450 °C	32
$CuWO_4$	codeposition of Cu_2O and WO_3 from an acidic aqueous bath	thermolysis at 500 °C in air	33
$CuWO_4$	cathodic deposition of WO_3	thermolysis in air at 550 °C in contact with copper(II) nitrate soln	34
Bi_2WO_6	same as above	same as above but with bismuth(III) nitrate solution used instead	34
$CuFeO_2$	cathodic codeposition of Cu and Fe from a DMSO bath	thermolysis at 650 °C in argon	35
$CuBi_2O_4$	cathodic codeposition of Cu and Bi in 1:2 ratio	thermolysis at 600 °C in air	36
$CuBi_2O_4$	anodic codeposition of CuO and Bi_2O_3 at 60 °C	thermolysis at 500 °C in air	37
Bi_2MoO_6	codeposition of Bi_2O_3 and MoO_3 in desired Bi:Mo ratio	thermolysis at 450 °C in air	38
$Cu_3V_2O_8$	nanoplatelets of $Cu_2(OH)_3Cl$ first prepared (see text)	the vanadate species are ion exchanged in the second step	28
$Ag_4V_2O_7$	two-step anodic stripping followed by precipitation (see text below)	$V_2O_7^{4-}$ chemically generated via slow acid hydrolysis (see text below)	29

- Myung, N.; Ham, S.; Choi, S.; Chae, Y.; Kim, W. G.; Jeon, Y. J.; Paeng, K. J.; Chanmanee, W.; de Tacconi, N. R.; Rajeshwar, K. Tailoring Interfaces for Electrochemical Synthesis of Semiconductor Films: $BiVO_4$, Bi_2O_3, or Composites. *J. Phys. Chem. C* **2011**, *115*, 7793−7800.[3] *This was a first demonstration that tailoring a support electrode−electrolyte interface could direct the electrosynthetic pathway toward a particular product.*
- Vali, A.; Jee, H. W.; Myung, N.; Rajeshwar, K. Combining Electrosynthesis with Thermolysis: A Safe/Scalable Route to Multinary Oxide Semiconductor Films. *ChemElectroChem* **2021**, *8*, 1251−1258.[4] *This study on a ternary silver vanadate demonstrated how electrosynthesis can be combined with thermosynthesis in a hybrid approach.*

1. INTRODUCTION AND SCOPE

1.1. Metal Oxides and Alloys

Metal oxides (MOs) display a remarkable range of electrical (electronic) and optical properties that make them intriguing candidates for both fundamental and applied studies.[1−4] Thus, they can be insulators, semiconductors, or even metallic conductors. Similarly, their optical absorption cross-section can range from nearly opaque to almost completely transparent,

https://doi.org/10.1021/acs.accounts.2c00838
Acc. Chem. Res. 2023, 56, 994−1003

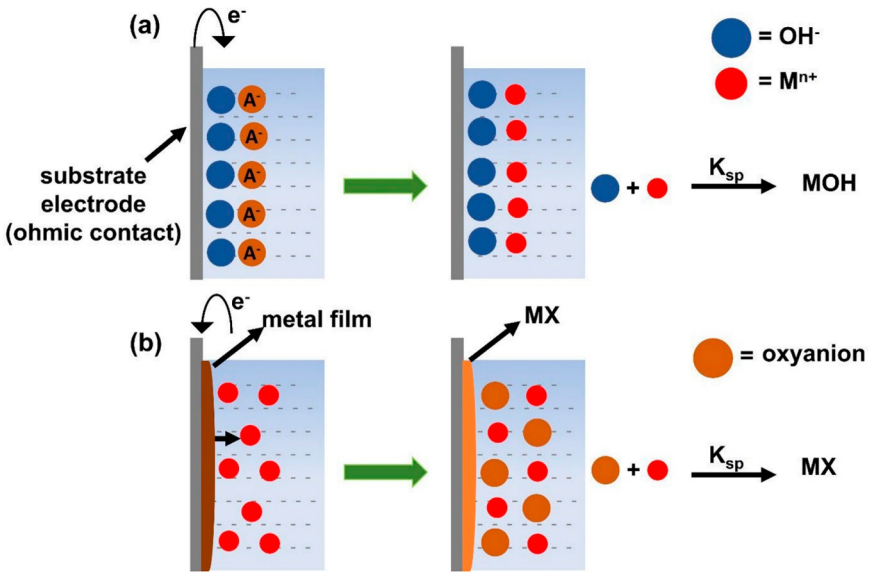

Figure 1. (a) Cathodic base electrogeneration; the (hydroxylated) MO precursor is simply shown here as MOH; the metal ion (shown here as M^{n+}) charge obviously will dictate the ultimate compound semiconductor stoichiometry. A^- is an anion (e.g., nitrate) whose electroreduction generates hydroxyl anions at the interface. (b) Two-step electrosynthesis variant developed in the Rajeshwar−Myung laboratories. The brown layer in the left frame is a zerovalent metal that can be electrochemically (anodically) stripped to afford the metal ions at the interphase for in situ precipitation (right frame). The MX layer thus formed is shown in orange color in the right frame. Once again, the MX compound stoichiometry is simplified (see also Tables 1 and 2.). The assumption here (and borne out by experiment) is that the stripping is complete and that there is no residual metal in admixture with the MX layer.

depending on their electronic band structures and doping profiles.[5] Here, we are mainly interested in MO semiconductors that have optical bandgaps in the ∼1−4 eV range; i.e., they respond mainly to the visible range of the electromagnetic spectrum. At the outset, it also is useful to differentiate the ultrathin, compact film that forms as a skin on metal surfaces ("native" oxide) vis-à-vis the thicker and morphologically more diverse counterparts that can be intentionally grown on metal surfaces (rather misleadingly termed, "thermal" oxide) (e.g., ref 6). We are interested in the latter type of oxides here. Finally, from a chemical perspective, it is important to recognize that MOs nominally are hydrated (or hydroxylated) to varying degrees depending on their growth history and exposure environments. Thus, the oxide formulas contained in Tables 1−3 most certainly do not reflect their surface composition or the hydrogen content. On the other hand, surface chemistries play a central role in materials behavior on both fundamental and technological levels.

Table 1 presents a compilation of binary MO semiconductors that have been electrosynthesized. The examples listed here (and in Tables 2 and 3 below) are not meant to be comprehensive but are representative only; more extensive compilations may be found elsewhere.[1,7] Table 2 contains the compilation of counterparts for ternary oxide semiconductors.

Most of the oxide compounds listed in Tables 1 and 2 occur as *n*-type semiconductors, but there are exceptions to this trend. Interestingly, Bi_2O_3 (Table 1) shows both *n*- as well as *p*-type behavior, as does BiOI (Table 2). On the other hand, Cu_2O is a *p*-type semiconductor. Claims of *n*-type semiconductor behavior for copper oxides appear to be problematic, as discussed elsewhere by one of us.[14] It is worth noting that the type of semiconductor conductivity (whether *n*- or *p*-type) can drive a particular technological application of the material.[15] For example, for solar water splitting, an *n*-type semiconductor functions as a photoanode, while a *p*-type semiconductor is used as a photocathode (to drive, for example, the reduction of protons to H_2 or CO_2 to value-added products).[7,15]

Not included for discussion in this Account are electronically conducting MOs that have been electrosynthesized, as reviewed elsewhere.[7] Many of these candidates (e.g., RuO_2, IrO_2) find applicability as electrocatalysts for technologically relevant processes, such as oxygen evolution reaction (OER) and hydrogen evolution reaction (HER) from water. Transparent conducting oxides (TCOs) form another class of metal oxides that have been examined from an electrosynthesis perspective.[5,7] The best known and most used oxides in this class are tin doped indium oxide (ITO) and fluorine doped tin oxide (FTO) coated on glass slides. These are heavily doped *n*-type semiconductors where the doping levels are increased to near degeneracy such that almost metallic conductivity is attained along with excellent optical transparency (see above). Less commercially developed yet are *p*-type TCOs whose conductivities and carrier mobilities are 1−2 orders of magnitude lower than their *n*-type counterparts and thus have considerable room for improvement. For example, this property gap has driven intense interest in delafossites of the type, $CuMO_2$, where M is a 3+ cation, e.g., Al, In, Ga. To the best of our knowledge, such oxides have not been electrosynthesized yet. On the other hand, metal vanadates, M_3VO_4 (M = Cu, Ag), which fall under the category of hole-conducting transparent oxides,[16] are indeed amenable to electrosynthesis as demonstrated by the Ag_3VO_4 example in Table 2. The Cu−Ag−O ternary phase diagram features an interesting hole-transporting compound, $AgCuO_2$,[17,18] wherein the charge is partially delocalized over the two cations. Two electrosynthesis studies have reported on this compound. In both studies,[18,19] $AgCuO_2$ nanoplates[18] or nanocrystalline films[19] were deposited on ITO[18] or FTO[19] glass slides from Ag(I)/Cu(II) ammoniacal aqueous solutions via interphasial pH control. We will return to the application of these materials in specific devices later in this Account.

https://doi.org/10.1021/acs.accounts.2c00838
Acc. Chem. Res. 2023, 56, 994−1003

Transparent conducting oxides provide a good introduction into MO alloys. Indeed, the distinction between very heavy "doping" (as in the case of TCOs) and alloys is rather murky. When the incorporation levels of the "foreign" atom(s) in the host amount to fractions of a mole percent (or even higher), we enter the regime of alloy formation. In the field of inorganic electrosynthesis, metal alloys have played a classical role spanning decades, as also amply discussed elsewhere in this special volume. However, MO alloys and, specifically, alloys of MO semiconductors have a much more recent history of the study.[20] Examples of solid solutions that have been electrosynthesized include $CuW_{1-x}Mo_xO_4$,[21] $Zn_{1-x}Cd_xO$,[22] and $Zn_{1-x}Co_xO$.[23]

2. ELECTROSYNTHESIS STRATEGIES

2.1. Cathodic Base Electrogeneration

This method already featured prominently in the library of MOs contained in Tables 1 and 2. Any cathodic electrochemical process that consumes protons (e.g., HER) or generates hydroxide species (e.g., electroreduction of nitrate or perchlorate anions) raises the ***local*** pH at the substrate electrode−electrolyte interface.[24] If the targeted metal cation M^{n+} (or combinations of cations in the case of ternary compounds or alloys, see above) is simultaneously present, the intrinsically low solubility products of metal hydroxides[25] can be exploited to selectively precipitate the metal hydroxide precursor product on the substrate surface (Figure 1a). The corresponding applicability to organic electrosynthesis has been discussed,[26] but is not relevant to this Account.

For the electrosynthesis of ternary MO semiconductors, a "hydroxy double salt", e.g., $Cu_2(OH)_3Cl$, has been electrogenerated using the metal chloride salt in an aqueous chloride medium containing *p*-benzoquinone for base generation.[7,27] The chloride in this precursor salt can be ion-exchanged with a target oxyanion (e.g., vanadate) as needed. This approach was used for the electrosynthesis of β-$Cu_3V_2O_8$.[28]

Subsequent conversion of the initial precursor to the targeted MO is usually accomplished via thermal routes, i.e., either by a postdeposition anneal or by performing the electrosynthesis at an elevated temperature (e.g., 50 °C) or a combination of both. The choice of these conditions has been largely arbitrary and is also driven by considerations related to the thermal stability of the metal oxide. Metal oxides do have the virtue of enhanced thermal stability (relative to other compounds such as chalcogenides), but it is all relative. For example, silver oxide compounds suffer from a rather poor thermal stability. Figure 2 contains results[29] illustrating this trend; the XRD data on electrosynthesized $Ag_4V_2O_7$ reveal thermal decomposition to $Ag_2V_4O_{11}$ and Ag at anneal temperatures higher than 150 °C.

In general, detailed thermal analyses performed under conditions mimicking MO electrosynthesis scenarios are conspicuously absent and are critically needed. More chemistry-specific spectroscopic (e.g., IR or Raman) tools on the MO precursor would also be very useful especially if they are performed in operando via a spectroelectrochemical mode (see below).[30]

2.2. Electrochemical Stripping Coupled with In Situ Precipitation

Instead of the metal ions present in the bulk electrolyte, they may be delivered to the substrate-electrolyte interphase in *precise, coulometrically controlled* amounts via anodic stripping (Figure 1b). Instead of OH^- species as in the base electrogeneration scheme considered above, subsequent generation of the final, targeted product relies on dosing of the deposition bath with the anionic species. This "two-step" electrosynthesis approach has been profitably employed in our laboratories as illustrated by the examples in Tables 1 and 2. Arguably, the first metal film deposition step in Figure 1b could be simply substituted with the use of the parent (bulk) metal anode instead (e.g., Bi, Ag, Cu) depending on the targeted MO. However, this defeats the possible use of the electrosynthesized product in optical, optoelectronic, or photoelectrochemical scenarios. In all of these cases, the initial metal phase must be optically transparent; this is facilitated by the initial cathodic deposition of the precursor metal film on a FTO or ITO surface (Figure 1b).

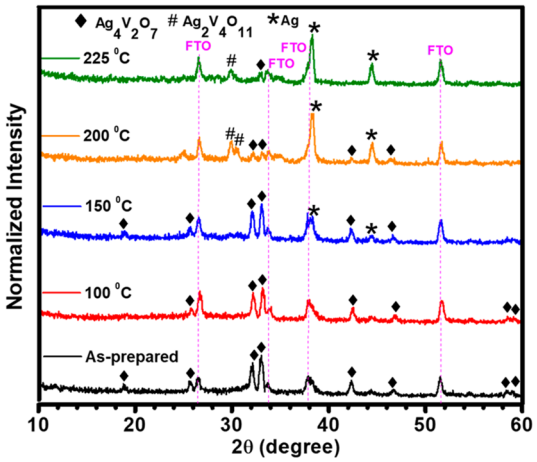

Figure 2. Thermal stability of electrosynthesized silver vanadate as probed by XRD. The temperatures shown refer to those under postdeposition film anneal. The substrate electrode (FTO) signals also manifest in these data, suggesting that the films are quite thin.

2.3. Anodic Oxidation of a Metal

In this approach,[24] a metal ion in a lower oxidation state is anodically converted to the corresponding species in a higher oxidation state. The medium pH is chosen such that the lower oxidation state is stable, while the higher oxidation state undergoes hydrolytic conversion to the metal hydroxide precursor or even the MO product. The anodic scheme has been mostly deployed for the electrosynthesis of conductive MOs (e.g., MnO_2)[24] and charge-storage or electrochromic MOs (e.g., NiO),[1,7] although examples do occur in the literature for MO *semiconductors* such as Fe_2O_3 and TiO_2 (Table 1).[7,8] The other anodic variant featured in Table 1 is performed at very high voltages (e.g., 10−30 V) under conditions instigating dielectric breakdown and breakup of the initial compact oxide film.[31] In favorable conditions, interesting morphologies for the MO product such as self-assembled NTAs (cf. Table 1) are obtained as elaborated later in this Account.

2.4. Hybrid Approaches

The synthetic scope of electrosynthesis can be further enhanced by incorporating other (nonelectrochemical) steps. This method is especially useful for the synthesis of ternary MOs. We already gleaned a hint of this with an ion exchange step following initial electrogeneration of the hydroxy double salt (see above).[28] In our laboratories, $CuVO_3$ was first prepared[4] via a two-step scheme, such as that in Figure 1b. Figure 3 (frames A−C) shows photographs of the $CuVO_3$ film for three values of

https://doi.org/10.1021/acs.accounts.2c00838
Acc. Chem. Res. 2023, 56, 994−1003

thickness; the film had a green hue (see above) and darkened as it became thicker.

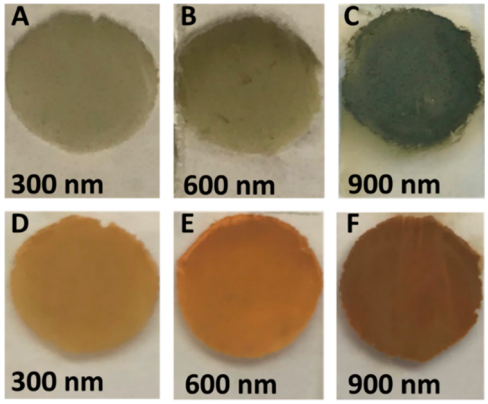

Figure 3. Photographs of (A–C) copper vanadate thin films after the second electrosynthesis step (cf., Figure 1b) and (D–F) samples after the third and final thermolysis step in air.

A third thermolysis step was incorporated to convert this product to $Cu_2V_2O_7$:

$$2CuVO_3 + 1/2O_2 \rightarrow Cu_2V_2O_7 \quad (1)$$

Thermal oxidation of the as-prepared film (Reaction 1) was accompanied by a color change from green to burnt orange. Photographs of the β-$Cu_2V_2O_7$ thin films with different thicknesses are shown in Figure 3, frames D–F. The initially green $CuVO_3$ phase was converted to a burnt orange β-$Cu_2V_2O_7$ by the final, electrothermodeposition (ETD) step. It is worth noting that this color change was observed only above 300 °C, guiding the specific choice of this thermolysis temperature. All the optical and optoelectronic data were consistent with these visual trends, as discussed elsewhere.[4]

The notion of enhancing the scope of electrosynthesis via hybrid strategies also extends to work in other laboratories.[28,32−38] Table 3 is a modified compilation of a version already presented in our companion study.[4] All these examples involve initial electrosynthesis of the two metal precursors in the ternary MO followed by a nonelectrochemical step that is most often thermal but can also be chemically derived as in ion exchange.

3. MECHANISTIC ASPECTS

Electrosynthesis undoubtedly has many attractive features as a synthesis candidate. However, a major handicap that it shares with all electrochemical experiments is that the information content is relatively limited to electrical parameters, such as current, potential, or charge. Specifically, electrosynthesis scenarios can be quite complex involving an interplay of adsorption, precipitation (cf., Figure 1), and processes that only involve redox conversion and charge transfer. Differentiation of these is readily accomplished by coupling the electrosynthesis set up with an in situ (operando) ultrasensitive mass probe such as electrochemical quartz crystal nanogravimetry (EQCN).[39−41] The coupled EQCN-linear sweep voltammetry (LSV)-coulometry setup has regularly been featured in the MO semiconductor electrosynthesis forays in our laboratories.[3,4,12,13,29]

Figure 4 exemplifies the type of data obtainable from the combination of LSV and EQCN with the Bi–V–O system as an example.[3] The interplay of variant interface parameters (e.g., pH, deposition potential, precursor chemistry) on whether Bi_2O_3 or $BiVO_4$ is formed can only be teased out with EQCN playing a complementary, operando role to LSV. Of course, ex situ tools such as XRD, XPS, laser Raman spectroscopy, etc., are equally valuable here, although certainly not timely in terms of information feedback as a combined (operando or in situ) probe. In this particular study, for example, in situ/operando LSV-EQCN data were complemented by ex situ XRD and XPS analyses of the product phases.[3]

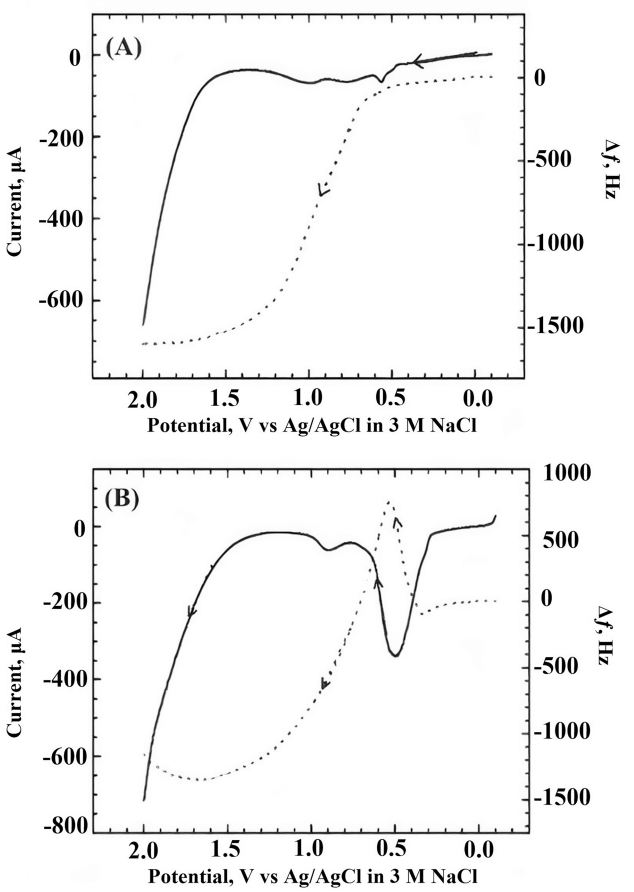

Figure 4. Examples for the combined use of LSV and EQCN for gleaning mechanistic insights into the two-step electrosynthesis of (A) $BiVO_4$ and (B) Bi_2O_3. Solid lines are LSV, and dashed lines are EQCN data. Note that a positive change in EQCN frequency signals mass loss, while a negative change signals mass uptake. The wave at ~0.5 V in (B) is from stripping of Bi from the premodified Pt/quartz sensor electrode. For electrolyte and other details, refer to ref 3. Adapted from ref 3. Copyright 2011 American Chemical Society.

The charge (Q) consumed during the voltammetric (LSV) scan can also be simultaneously assayed in an LSV-EQCN experiment. The combination of Q with the EQCN-derived frequency shift ($-\Delta f$) affords an estimation of the electron stoichiometry, n via the Sauerbrey equation.[39−41] Figure 5 presents five examples of such "Sauerbrey plots" taken from our recent electrosynthesis studies[4,12,13,28] of silver and copper vanadates. The n values computed from the plot slopes in Figure 5 show satisfactory conformity (within experimental uncertainty) with those expected from the postulated pathway, as shown in Table 4. Thus, the ordinate in Figure 6 directly scales with the n value. The initial deviation of the plot for Cu from linearity is readily rationalized by the one-electron conversion of

https://doi.org/10.1021/acs.accounts.2c00838
Acc. Chem. Res. 2023, 56, 994−1003

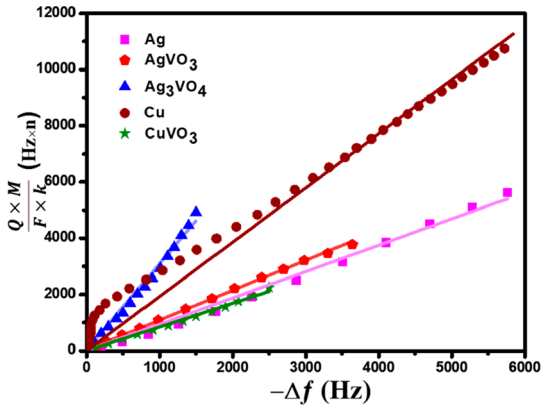

Figure 5. Sauerbrey plots for the processes are shown in Table 4. The lines are least-squares fits of the data points.

Table 4. Electron Stoichiometries Derived from Sauerbrey Analyses

electrochemical pathway	expected *n* value	measured *n* value[a]	ref
$Ag^+ + e^- \rightarrow Ag$	1	0.94	13
$3Ag_{(s)} \rightarrow 3Ag^+_{(aq)} + 3e^-$	3	3.05	12
$Ag + VO_3^- \rightarrow AgVO_3 + e^-$	1	1.06	13
$Cu^{2+} + 2e^- \rightarrow Cu$	2	1.93	4
$Cu + VO_3^- \rightarrow CuVO_3 + e^-$	1	0.86	4

[a]Corresponding plots from which these values were derived are in Figure 6 (see text).

Cu to Cu(I) species—a process that consumes charge but is not accompanied by mass loss.

It is worth noting that in some cases in the two-step electrosynthesis scheme as exemplified by the initial electrodeposition of metallic silver, a nonaqueous medium was employed.[12,13] This was done as a precautionary measure against the electrogeneration of silver oxide phases that would have conspired against the second (ternary MO precipitation) step (cf., Figure 1b). This complication does not exist with the copper-based MO cases. Also worthy of note is that both the classical base electrogeneration and our two-step schemes are predicated on the very low solubility products reported for MOs and metal vanadates. However, the literature values for the solubility products, K_{sp} (cf., Figure 1) pertain to *homogeneous* situations. Do these values shift under the very high electric fields extant at electrode−electrolyte interfaces? This hitherto uncharted territory demands future studies; nonetheless, we may expect the values to shift even lower when the activities of the participating ionic partners (e.g., Cu^+, VO_3^-) in precipitation processes at electrode−electrolyte *interphases* are considered.

The targeted anionic species needed for the second precipitation step can be generated by manipulating the solution chemistry. Thus, our electrosynthesis of $Ag_4V_2O_7$ demands dimeric $V_2O_7^{4-}$ species that can be generated by diffusing CO_2 through the initial sodium orthovanadate (Na_3VO_4) solution followed by a month-long aging period during which the pH gradually decreases (Figure 6, left), consistent with reaction of orthovanadate species with the carbonic acid-generated protons:

$$2VO_4^{3-} + 2H^+ \rightarrow V_2O_7^{4-} + H_2O \qquad K_{eq} = 6.0 \times 10^{27} \tag{2}$$

Further details are given in ref 29. The two-step electrosynthesis of $Ag_4V_2O_7$ proceeds via Reactions 3 and 4:[29]

$$Ag_{(s)} \rightarrow Ag^+_{(aq)} + e^- \qquad E^0 = +0.800\ \text{V vs NHE} \tag{3}$$

$$4Ag^+_{(aq)} + V_2O_7^{4-}{}_{(aq)} \rightarrow Ag_4V_2O_{7(s)} \qquad K_{sp} = 2.0 \times 10^{-14} \tag{4}$$

Another example of manipulating solution chemistry is the hydrolytic conversion of the VO_3^- precursor to the desired VO_4^- species in the two-step electrosynthesis of $BiVO_4$.[3]

Closer examination of the data in Figure 4B shows an uptick (reversal) in the EQCN frequency change at potentials higher than 1.5 V. Note that this feature is not present in the corresponding data in Figure 5A.[3] Although not addressed in ref 3, we suspect that this mass loss arises from anodic corrosion of the electrosynthesized Bi_2O_3 layer.

4. MORPHOLOGICAL ASPECTS

The classical anodic oxide films on metal surfaces (whether they are native or thermal) are relatively compact, although they may not be nanoscopically smooth.[8] In contrast, those grown at high voltages have distinct morphologies, either nanoporous or nanotubular, depending on a variety of factors beyond the scope of this Account. Securing high surface areas may be a prerequisite for many applications, for example, solar energy conversion (e.g., photovoltaic or photoelectrochemical) or energy storage (electrochemical capacitor), to mention two.

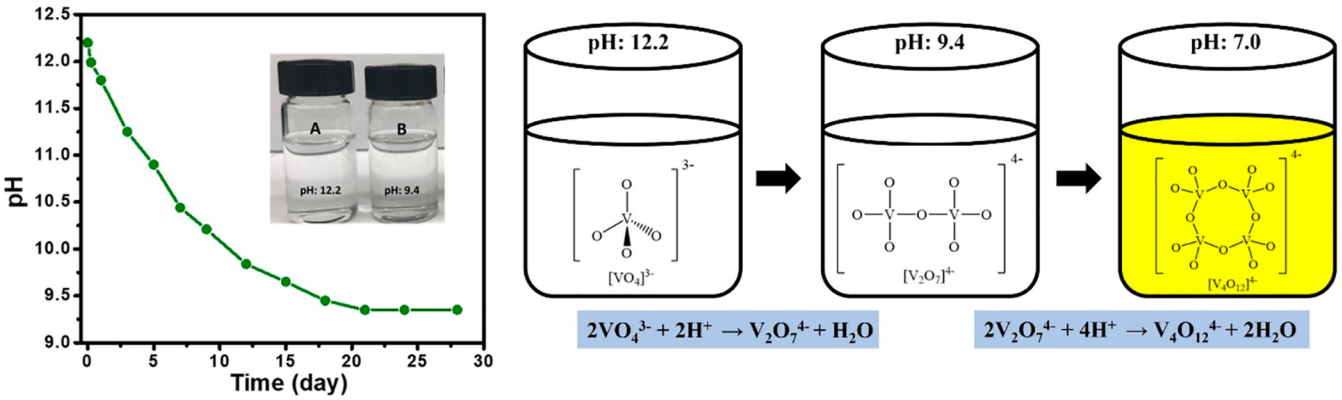

Figure 6. Solution pH vs time during the aging of Na_3VO_4 solution (left); the inset captures photos of the solutions at the extremities of the pH swing. The plateau signals the balance between proton generation (via carbonic acid dissociation) and proton consumption, as shown in Reaction 2. The right frames show the vanadate speciation change with solution pH.

https://doi.org/10.1021/acs.accounts.2c00838
Acc. Chem. Res. 2023, 56, 994−1003

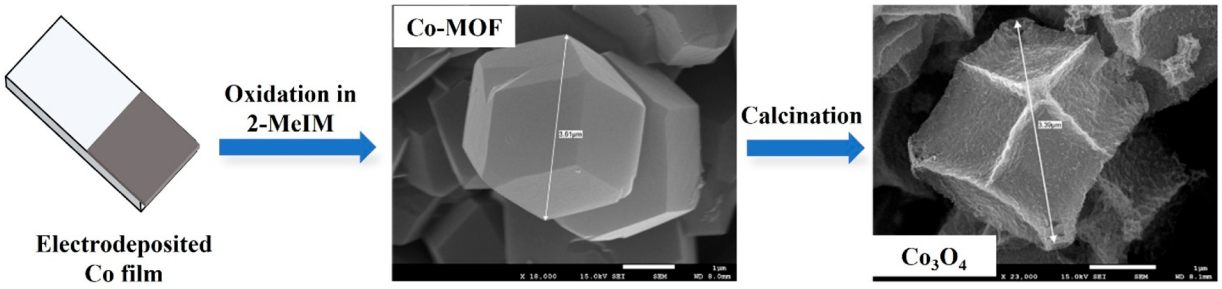

Figure 7. A cobalt-modified FTO electrode is converted to a cobalt-MOF electrode by anodic oxidation in an aqueous 2-methylimidazole (2-MeIM) medium and subsequently calcined to afford cobalt oxide. Further details may be found in ref 45. Adapted with permission from ref 45. Copyright 2020 American Chemical Society.

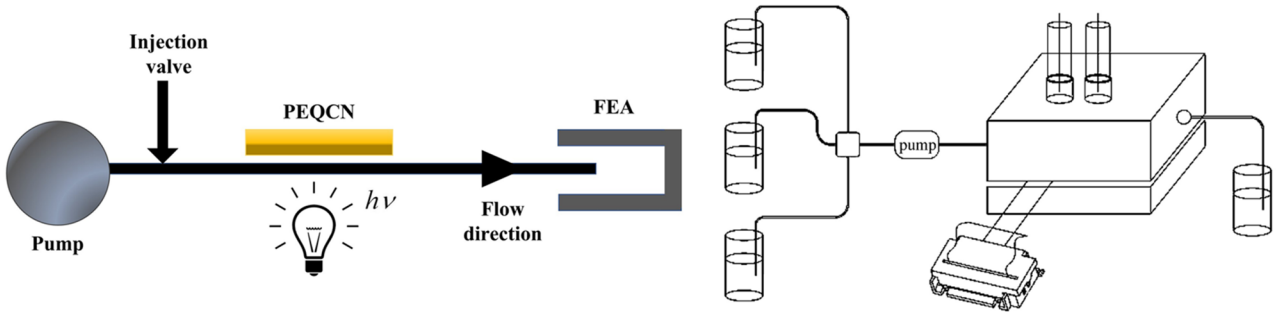

Figure 8. (a) Flow electrosynthesis coupled with EQCN and (b) our previous adaptation of the flow mode for the study of electrosynthesized bismuth telluride (see the text).

Others (e.g., optoelectronic devices such as lasers) demand the structural conformity of the electrosynthesized layer with the underlying substrate, i.e., epitaxial growth. Examples of epitaxial MO growth include ZnO/GaN and Cu_2O on a variety of surfaces as reviewed elsewhere by one of us.[1]

Preferred grain orientation during electrosynthesis is another aspect that has been studied intensely, especially for binary MOs such as Cu_2O, both in our laboratories[42] and elsewhere.[1] Binary MOs such as ZnO and Cu_2O have been popular candidates for exploring shape control of the grains within the electrodeposited films.[1,7] The proclivity of electrosynthesis approaches to generate nontargeted phases (see above) can be exploited here. For example, excess Zn is often found in cathodically electrosynthesized ZnO. However, this "nuisance" phase can be galvanically replaced with Au to electrosynthesize a composite Au/ZnO nanodot array (NDA).[43]

Galvanic displacement is a versatile approach in inorganic electrosynthesis, as amply discussed elsewhere in this special volume. Within the narrower context of MO semiconductor electrosynthesis, however, this approach can be profitably combined with the photoinduced deposition of another layer (e.g., a metal chalcogenide) on top of the parent MO surface. Thus, as in the above Au/ZnO example, we exploited the excess Zn in the initially electrosynthesized ZnO NDA with Se.[44] Finally, the Se precursor species on the ZnO surface were converted to CdSe via photocathodic deposition to ultimately afford a ZnO/CdSe composite.[44] As discussed in the original paper, such composites are of interest when the rather high energy band gap of ZnO must be overcome via "visible light sensitization". The CdSe component serves as a sensitizer in this case; such sensitized composites are relevant to photovoltaic and photocatalytic applications.[44]

Clearly, the above examples provide further demonstration of the versatility of interfacial chemistry tuning in MO electrosynthesis scenarios beyond what is presented in Section 1 of this Account. The final aspect in this section concerns the use of templates to direct the morphology in electrosynthesis scenarios. Our laboratories have decade-long activity in this area; one recent example[45] is illustrated by the data in Figure 7. In this study,[45] electrosynthesis of a cobalt metal−organic framework (MOF) was used to direct the subsequent formation of cobalt oxide (Co_3O_4) or cobalt selenide (CoSe). The morphological aspects of the oxide conversion progression are shown in Figure 7. Although neither Co_3O_4 nor CoSe are semiconductors, extension of these ideas to MO electrosynthesis scenarios seems to be straightforward.

As a final example of morphologic tuning, a double-template approach,[47] using initially polystyrene nanospheres and subsequently a polypyrrole conducting polymer template, was used to electrosynthesize the NDAs on the Au surface.[46]

5. BACK TO THE FUTURE: FLOW ELECTROSYNTHESIS/ANALYSIS AND EXOTIC ELECTROSYNTHESIS SCENARIOS

We envision that stability issues associated with electrosynthesized MO layers can be effectively addressed by a flow scheme, as sketched in Figure 8. The setup shown also incorporates an illumination module for performing photoelectrochemical experiments, the principle remains essentially the same in both the "light" and "dark" experimental scenarios. Any (corrosion-generated) species emanating from the (photo)electrosynthesized MO layer will be swept into the flow stream to a downstream electroanalytical (or ICP-MS) detector. Anodic or cathodic photocorrosion of the MO will generate soluble species that are swept downstream to the detector where

https://doi.org/10.1021/acs.accounts.2c00838
Acc. Chem. Res. 2023, 56, 994−1003

they can be detected and quantified. There is precedence for this flow approach for studying semiconductor photocorrosion (including MO electrodes) albeit not in an electrosynthesis setting (for example, ref 48).

Our own foray into flow electroanalysis (FEA) began earlier with the assay of electrosynthesized CdSe upstream.[49] Another relevant study concerned the FEA of electrosynthesized bismuth telluride (Figure 8b).[50] Unfortunately, space constraints prohibit a fuller discussion, and we refer to the original papers on this topic.[49,50] A flow mode for the QCN technique is not new, and indeed, commercial equipment is now available to implement this. Indeed, we anticipate that many of the future advances in MO electrosynthesis are likely to feature new ways of incorporating mechanistic and morphological probes (e.g., XPS, Auger or positron-based spectroscopies, and scanning tunneling, atomic force, or electrochemical microscopies) in a MO electrosynthesis setting. Spectroelectrochemical approaches[30] have immense appeal in an operando context; many examples already exist for their ability to provide mechanistic information that are relevant in an operating (photo)electrochemical cell (for example, refs 51−54). Further application to MO electrosynthesis surely lies around the corner.

We close this Account with another innovation that enhances the scope of MO electrosynthesis, namely, the use of "exotic" environments such as ionic liquids[55] or MOFs.[56] For example, can we enhance the performance and stability of MO nanoparticles derived from a "ship in a bottle" chemical synthesis paradigm (see ref 57) using such environments? In this scenario, the host framework imparts improved (photo)-electrochemical activity or stability to the electrosynthesized assembly.

6. CONCLUSIONS AND OUTLOOK

Hopefully, the foregoing has afforded perspectives on the power of electrosynthesis strategies for preparing MO semiconductor frameworks for a variety of targeted applications. This topic and the addressed materials in this Account represent a very rich tapestry of possibilities for doing both fundamental and applied science. Specifically, there is immense scope for innovating new strategies that will further improve materials' performance, for example, for generation of solar fuels. This performance gap and the attendant challenges have been articulated by us elsewhere.[58] Nonetheless, the future role of electrosynthesis with or without assistance from light or flow modes remains bright.

AUTHOR INFORMATION

Corresponding Author

Krishnan Rajeshwar − *Department of Chemistry & Biochemistry, The University of Texas at Arlington, Arlington, Texas 76019-0065, United States;* orcid.org/0000-0003-4917-7790; Email: rajeshwar@uta.edu

Authors

Abbas Vali − *Department of Chemistry & Biochemistry, The University of Texas at Arlington, Arlington, Texas 76019-0065, United States*

Abhishek Rawat − *Department of Chemistry & Biochemistry, The University of Texas at Arlington, Arlington, Texas 76019-0065, United States*

Noseung Myung − *Department of Applied Chemistry, Konkuk University Glocal Campus, Chungju, Chungbuk 27478, Republic of Korea*

Complete contact information is available at: https://pubs.acs.org/10.1021/acs.accounts.2c00838

Author Contributions

CRediT: **Krishnan Rajeshwar** conceptualization (equal), data curation (equal), funding acquisition (equal), project administration (equal), supervision (equal), writing-original draft (equal), writing-review & editing (equal); **Noseung Myung** formal analysis (equal), investigation (equal), methodology (equal), software (equal), supervision (equal), writing-review & editing (equal); **Abbas Vali** data curation (equal), investigation (equal), methodology (equal), software (equal), validation (equal); **Abhishek Rawat** data curation (equal), formal analysis (equal), software (equal), writing-review & editing (equal).

Notes

The authors declare no competing financial interest.

Biographies

Dr. Rajeshwar is a Distinguished University Professor at the University of Texas at Arlington. He is also the founding director of the Center for Renewable Energy Science & Technology (CREST) on campus. He was elected Vice President of the Electrochemical Society (ECS) and is a past President of the ECS. He is a past Editor of the ECS *Interface* and currently serves on the editorial boards of several electrochemical journals. He is currently the Editor-in-Chief of the ECS *Journal of Solid-State Science & Technology*. After postdoctoral training at Colorado State University, he joined UT Arlington in 1983. His research interests span a wide spectrum and include photoelectrochemistry; solar energy conversion; renewable energy; materials chemistry; semiconductor electrochemistry; and environmental chemistry.

Dr. Noseung Myung is a Professor in the Department of Applied Chemistry at Konkuk University Glocal Campus, South Korea. He received Ph.D. from the University of Texas at Arlington under the direction of Prof. Krishnan Rajeshwar. His current research focuses on the electrosynthesis of metal chalcogenides and the use of EQCN for a better understanding of electrodeposition mechanisms.

Dr. Abbas Vali received his Ph.D. in chemistry from the University of Texas at Arlington (UTA) under the supervision of Prof. Krishnan Rajeshwar. His current research interests focus on electrosynthesis and photoelectrochemistry of ternary oxide semiconductors. He is now completing his postdoctoral fellowship under supervision of Prof. Sherri A. McFarland in UTA.

Mr. Abhishek Rawat earned his master's degree from Jawaharlal Nehru Center for Advanced Scientific Research (JNCASR) in 2020. At present, he is a second-year Ph.D. candidate in Prof. Rajeshwar's Laboratory. His current research interest lies in the design and optimization of oxide semiconductors for solar fuels generation and in structure-composition correlations of chemical and optoelectronic properties of semiconductors and alloys.

ACKNOWLEDGMENTS

Past support of the work in the Rajeshwar laboratory by the U.S. Department of Energy (Basic Energy Sciences Program) and the National Science Foundation (Chemistry Division) is acknowledged. Our current efforts are supported by NSF-PREM (Grant DMR-2122128). Research funding in the Myung group was provided by the Basic Science Research Program through the National Research Foundation of Korea (NRF), Ministry of Education (Grant NRF-2016R1D1A1B02010133). Finally, we thank three anonymous reviewers for their constructive criticisms of an earlier manuscript draft.

REFERENCES

(1) Schlesinger, T. E.; Rajeshwar, K.; de Tacconi, N. R.; Electrodeposition of Semiconductors. In *Modern Electroplating*; Schlesinger, M., Ed.; Springer: New York, 2010; Chapter 14, pp 383−411.

(2) Yamamoto, J.; Tan, A.; Shiratsuchi, R.; Hayase, S.; Chenthamarakshan, C. R.; Rajeshwar, K. A 4% Dye-Sensitized Solar Cell Fabricated from Cathodically Electrosynthesized Composite Titania Films. *Adv. Mater.* **2003**, *15*, 1823−1825.

(3) Myung, N.; Ham, S.; Choi, S.; Chae, Y.; Kim, W. G.; Jeon, Y. J.; Paeng, K. J.; Chanmanee, W.; de Tacconi, N. R.; Rajeshwar, K. Tailoring Interfaces for Electrochemical Synthesis of Semiconductor Films: $BiVO_4$, Bi_2O_3, or Composites. *J. Phys. Chem. C* **2011**, *115*, 7793−7800.

(4) Vali, A.; Jee, H. W.; Myung, N.; Rajeshwar, K. Combining Electrosynthesis with Thermolysis: A Safe/Scalable Route to Multinary Oxide Semiconductor Films. *ChemElectroChem.* **2021**, *8*, 1251−1258.

(5) Cerqueira, T. F. T.; Lin, S.; Amsler, M.; Goedecker, S.; Botti, S.; Marques, M. A. L. Identification of Novel Cu, Ag, and Au Ternary Oxides from Global Structural Prediction. *Chem. Mater.* **2015**, *27*, 4562−4573.

(6) Morita, M.; Ohmi, T.; Hasegawa, E.; Kawakami, M.; Ohwada, M. Growth of Native Oxide on a Silicon Surface. *J. Appl. Phys.* **1990**, *68*, 1272−1281.

(7) Kang, D.; Kim, T. W.; Kubota, S. R.; Cardiel, A. C.; Cha, H. G.; Choi, K. S. Electrochemical Synthesis of Photoelectrodes and Catalysts for Use in Solar Water Splitting. *Chem. Rev.* **2015**, *115*, 12839−12887.

(8) Kavan, L.; O'Regan, B.; Kay, A.; Grätzel, M. Preparation of TiO_2 (Anatase) Films on Electrodes by Anodic Oxidative Hydrolysis of $TiCl_3$. *J. Electroanal. Chem.* **1993**, *346*, 291−307.

(9) Schrebler, R.; Bello, K.; Vera, F.; Cury, P.; Muñoz, E.; Del Río, R.; Gómez Meier, H.; Córdova, R.; Dalchiele, E. A. An Electrochemical Deposition Route for Obtaining α-Fe_2O_3 Thin Films. *Electrochem. Solid-State Lett.* **2006**, *9*, C110.

(10) Nagarajan, N.; Zhitomirsky, I. Cathodic Electrosynthesis of Iron Oxide Films for Electrochemical Supercapacitors. *J. Appl. Electrochem.* **2006**, *36*, 1399−1405.

(11) Roy, D.; Samu, G. F.; Hossain, M. K.; Janáky, C.; Rajeshwar, K. On the Measured Optical Bandgap Values of Inorganic Oxide Semiconductors for Solar Fuels Generation. *Catal. Today* **2018**, *300*, 136−144.

(12) Vali, A.; Toth, P. S.; Jee, H. W.; Firouzan, F.; Janáky, C.; Paeng, K. J.; Myung, N.; Rajeshwar, K. Electrosynthesis and Properties of Crystalline and Phase-Pure Silver Orthovanadate. *J. Phys. Chem. C* **2020**, *124*, 19980−19989.

(13) Vali, A.; Sarker, H. P.; Jee, H. W.; Kormányos, A.; Firouzan, F.; Myung, N.; Paeng, K. J.; Huda, M. N.; Janáky, C.; Rajeshwar, K. Electrodeposition of Silver Vanadate Films: A Tale of Two Polymorphs. *ChemPhysChem* **2019**, *20*, 2635−2646.

(14) Firouzan, F.; Vali, A.; Rajeshwar, K. Editors' Choice—Perspective—Bipolar Photoactivity: The Anomalous Case of Electrodeposited Copper Oxide Films. *J. Electrochem. Soc.* **2020**, *167*, 136505.

(15) Oliveira, J. A.; Silva, R. R. M.; da Silva, G. T. S. T.; Torres, J. A.; Vali, A.; Ribeiro, C.; Rajeshwar, K.; Ruotolo, L. A. M. Copper Vanadates: Targeted Synthesis of Two Pure Phases and Use in a Photoanode/Cathode Setup for Selective Photoelectrochemical Conversion of Carbon Dioxide to Liquid Fuel. *Mater. Res. Bull.* **2022**, *149*, 111716.

(16) Trimarchi, G.; Peng, H.; Im, J.; Freeman, A. J.; Cloet, V.; Raw, A.; Poeppelmeier, K. R.; Biswas, K.; Lany, S.; Zunger, A. Using Design Principles to Systematically Plan the Synthesis of Hole-Conducting Transparent Oxides: Cu_3VO_4 and Ag_3VO_4 as a Case Study. *Phys. Rev. B - Condens. Matter Mater. Phys.* **2011**, *84*, 1−14.

(17) Muñoz-Rojas, D.; Fraxedas, J.; Gómez-Romero, P.; Casañ-Pastor, N. Room Temperature Solid-State Transformation from $Ag_2Cu_2O_3$ to $Ag_2Cu_2O_4$ by Ozone Oxidation. *J. Solid State Chem.* **2005**, *178*, 295−305.

(18) Lu, Q.; Lu, K.; Zhang, L.; Gong, J.; Liu, R. Electrodeposition of $AgCuO_2$ Nanoplates. *J. Electrochem. Soc.* **2017**, *164*, D130−D134.

(19) Shi, J.; Li, B.; Zhang, Q.; Rui, Y. Electrodeposited Ternary $AgCuO_2$ Nanocrystalline Films as Hole Transport Layers for Inverted Perovskite Solar Cells. *J. Alloys Compd.* **2022**, *890*, 161879.

(20) Rawat, A.; Clark, L. M.; Zhang, C.; Cavin, J.; Riddhi Ananth, R.; Goldfine, E.; Sangwan, V. K.; Toth, P. S.; Janáky, C.; Bedzyk, M. J.; Weiss, E. A.; Rondinelli, J. M.; Hersam, M. C.; Meletis, E. I.; Rajeshwar, K., Solution Combustion Synthesis and Characterization of Magnesium Copper Vanadates. *Inorg. Chem.*, first cycle review completed.

(21) Hill, J. C.; Ping, Y.; Galli, G. A.; Choi, K. S. Synthesis, Photoelectrochemical Properties, and First Principles Study of *n*-Type $CuW_{1-x}Mo_xO_4$ Electrodes Showing Enhanced Visible Light Absorption. *Energy Environ. Sci.* **2013**, *6*, 2440−2446.

(22) Yogeeswaran, G.; Chenthamarakshan, C. R.; Seshadri, A.; de Tacconi, N. R.; Rajeshwar, K. Cathodic Electrodeposition in the Ternary Zn-Cd-O System: Mixed $(ZnO)_x(CdO)_{1-x}$ Film Formation versus Cd-Doping of ZnO Films. *Thin Solid Films* **2006**, *515*, 2464−2470.

(23) Jaramillo, T. F.; Baeck, S. H.; Kleiman-Shwarsctein, A.; Choi, K. S.; Stucky, G. D.; McFarland, E. W. Automated Electrochemical Synthesis and Photoelectrochemical Characterization of $Zn_{1-x}Co_xO$ Thin Films for Solar Hydrogen Production. *J. Comb. Chem.* **2005**, *7*, 264−271.

(24) Therese, G. H. A.; Kamath, P. V. Electrochemical Synthesis of Metal Oxides and Hydroxides. *Chem. Mater.* **2000**, *12*, 1195−1204.

(25) Harris, D. C. *Quantitative Chemical Analysis*, 7th ed.; W. H. Freeman and Company: New York, 2007.

(26) Cheng, S.; Hawley, M. D. Electrogenerated Bases: The Role of Weak Electroinactive Proton Donors and the Effect of Electrocatalysis on the Redox Behavior of Azobenzene. *J. Org. Chem.* **1985**, *50*, 3388−3392.

(27) Cardiel, A. C.; McDonald, K. J.; Choi, K. S. Electrochemical Growth of Copper Hydroxy Double Salt Films and Their Conversion to Nanostructured *p*-Type CuO Photocathodes. *Langmuir* **2017**, *33*, 9262−9270.

(28) Tang, D.; Zhong, S. Communication—Preparation of a Porous β-$Cu_3V_2O_8$ Film for Photoelectrochemical Water Oxidation. *J. Electrochem. Soc.* **2021**, *168* (6), 066509.

(29) Vali, A.; Kim, S. Y.; Danladi, F.; Rawat, A.; Zhang, C.; Toth, P. S.; Janáky, C.; Myung, N.; Meletis, E. I.; Rajeshwar, K. Hybrid Cathodic/Anodic Electrosynthesis of Phase Pure $Ag_4V_2O_7$ Thin Films. *J. Electrochem. Soc.*, submitted.

(30) Rajeshwar, K.; Lezna, R. O.; de Tacconi, N. R. Light in an Electrochemical Tunnel? Solving Analytical Problems in Electrochemistry via Spectroscopy. *Anal. Chem.* **1992**, *64*, 429A−441A.

(31) Ham, D.; Mishra, K. K.; Rajeshwar, K. Anodic Electrosynthesis of Cadmium Selenide Thin Films : Characterization and Comparison with the Passive/Transpassive Behavior of the Counterparts. *J. Electrochem. Soc.* **1991**, *138*, 100−108.

(32) Kang, D.; Park, Y.; Hill, J. C.; Choi, K. Preparation of Bi-Based Ternary Oxide Photoanodes $BiVO_4$, Bi_2WO_6, and $Bi_2Mo_3O_{12}$ Using Dendritic Bi-Metal Electrodes. *J. Phys. Chem. Lett.* **2014**, *5*, 2994−2999.

(33) Yourey, J. E.; Bartlett, B. M. Electrochemical Deposition and Photoelectrochemistry of $CuWO_4$, a Promising Photoanode for Water Oxidation. *J. Mater. Chem.* **2011**, *21*, 7651−7660.

(34) Hill, J. C.; Choi, K. S. Synthesis and Characterization of High Surface Area $CuWO_4$ and Bi_2WO_6 Electrodes for Use as Photoanodes for Solar Water Oxidation. *J. Mater. Chem. A* **2013**, *1*, 5006−5014.

(35) Read, C. G.; Park, Y.; Choi, K. S. Electrochemical Synthesis of *p*-Type $CuFeO_2$ Electrodes for Use in a Photoelectrochemical Cell. *J. Phys. Chem. Lett.* **2012**, *3*, 1872−1876.

(36) Hahn, N. T.; Holmberg, V. C.; Korgel, B. A.; Mullins, C. B. Electrochemical Synthesis and Characterization of *p*-$CuBi_2O_4$ Thin Film Photocathodes. *J. Phys. Chem. C* **2012**, *116*, 6459−6466.

(37) Nakabayashi, Y.; Nishikawa, M.; Nosaka, Y. Fabrication of $CuBi_2O_4$ Photocathode through Novel Anodic Electrodeposition for Solar Hydrogen Production. *Electrochim. Acta* **2014**, *125*, 191−198.

(38) Zheng, F. L.; Li, G. R.; Yu, X. L.; Tong, Y. X. Synthesis of Bismuth Molybdate Nanowires via Electrodeposition-Heat-Treatment Method. *Electrochem. Solid-State Lett.* **2009**, *12*, K56.

https://doi.org/10.1021/acs.accounts.2c00838
Acc. Chem. Res. 2023, 56, 994−1003

(39) Ham, S.; Jeon, S.; Park, M.; Choi, S.; Paeng, K. J.; Myung, N.; Rajeshwar, K. Electrodeposition and Stripping Analysis of Bismuth Selenide Thin Films Using Combined Electrochemical Quartz Crystal Microgravimetry and Stripping Voltammetry. *J. Electroanal. Chem.* **2010**, *638*, 195−203.
(40) Deakin, M. R.; Buttry, D. A. Electrochemical Applications of the Quartz Crystal Microbalance. *Anal. Chem.* **1989**, *61*, 1147A−1154A.
(41) Buttry, D. A. *Electroanalytical Chemistry*; Bard, A. J., Ed.; Marcel Dekker: New York, 1991; Vol. *17*, pp 1−85.
(42) Wang, L. C.; de Tacconi, N. R.; Chenthamarakshan, C. R.; Rajeshwar, K.; Tao, M. Electrodeposited Copper Oxide Films: Effect of Bath pH on Grain Orientation and Orientation-Dependent Interfacial Behavior. *Thin Solid Films* **2007**, *515*, 3090−3095.
(43) Myung, N.; Choi, S.; Lee, W.; Jeong, S.; Rajeshwar, K. Synthesis of Au/ZnO Composite Nanorod Arrays via Electrodeposition Followed by Galvanic Replacement. *ECS Electrochem. Lett.* **2013**, *2*, D33.
(44) Choi, S.; Chae, Y.; Ham, S.; Lee, W.; Myung, N.; Rajeshwar, K. CdSe/ZnO Composite via Galvanic Displacement Followed by Photocathodic Deposition: Hybrid Electrosynthesis and Characterization. *J. Phys. Chem. C* **2012**, *116*, 20146−20153.
(45) Jee, H.-W.; Paeng, K.-J.; Myung, N.; Rajeshwar, K. Electrochemical Deposition of a Metal-Organic Framework and Subseqeunt Conversion to Cobalt Selenide. *ACS Appl. Electron. Mater.* **2020**, *2*, 1358−1364.
(46) Choi, B. B.; Myung, N.; Rajeshwar, K. Double Template Electrosynthesis of ZnO Nanodot Array. *Electrochem. Commun.* **2007**, *9*, 1592−1595.
(47) Ghanem, M. A.; Bartlett, P. N.; De Groot, P.; Zhukov, A. A Double Templated Electrodeposition Method for the Fabrication of Arrays of Metal Nanodots. *Electrochem. Commun.* **2004**, *6*, 447−453.
(48) Knöppel, J.; Zhang, S.; Speck, F. D.; Mayrhofer, K. J. J.; Scheu, C.; Cherevko, S. Time-Resolved Analysis of Dissolution Phenomena in Photoelectrochemistry—A Case Study of WO_3 Photocorrion. *Electrochem. Commun.* **2018**, *96*, 53−56.
(49) Myung, N.; Wei, C.; Rajeshwar, K. Flow Electroanalysis of Compound Semiconductor Thin Films: Application to the Compositional Assay of Cathodically Electrosynthesized Cadmium Selenide. *Anal. Chem.* **1992**, *64*, 2701−2705.
(50) Ham, S.; Jeon, S.; Lee, U.; Park, M.; Paeng, K. J.; Myung, N.; Rajeshwar, K. Compositional Analysis of Electrodeposited Bismuth Telluride Thermoelectric Thin Films Using Combined Electrochemical Quartz Crystal Microgravimetry-Stripping Voltammetry. *Anal. Chem.* **2008**, *80*, 6724−6730.
(51) Zegkinoglou, I.; Zendegani, A.; Sinev, I.; Kunze, S.; Mistry, H.; Jeon, H. S.; Zhao, J.; Hu, M. Y.; Alp, E. E.; Piontek, S.; Smialkowski, M.; Apfel, U.-P.; Kormann, F.; Neugebauer, J.; Hickel, T.; Roldan Cuenya, B. *Operando* Phonon Studies of the Protonation Mechanism in Highly Active Hydrogen Evolution Reaction Pentlandite Catalysts. *J. Am. Chem. Soc.* **2017**, *139*, 14360−14363.
(52) Firet, N. J.; Blommaert, M. A.; Burdyny, T.; Venugopal, A.; Bohra, D.; Longo, A.; Smith, W. A. *Operando* EXAFS Study Reveals Presence of Oxygen in Oxide-Derived Silver Catalysts for Electrochemical CO_2 Reduction. *J. Mater. Chem. A* **2019**, *7*, 2597−2607.
(53) Gao, J.; Zhang, H.; Guo, X.; Luo, J.; Zakeeruddin, S. M.; Ren, D.; Grätzel, M. Selective C-C Coupling in Carbon Dioxide Electroreduction via Efficient Spilloevr of Intermediates As Supported by Operando Raman Spectroscopy. *J. Am. Chem. Soc.* **2019**, *141*, 18704−18714.
(54) Mesa, C. A.; Francàs, L.; Yang, K. R.; Garrido-Barros, P.; Pastor, E.; Ma, Y.; Kafizas, A.; Rosser, T. E.; Mayer, M. T.; Reisner, E.; Grätzel, M.; Batista, V. S.; Durrant, J. R. Multihole Water Oxidation Catalysis on Haematite Photoanodes Revealed by Operando Soectroelectrochemistry and DFT. *Nat. Chem.* **2020**, *12*, 82−89.
(55) Shah, N. K.; Pati, R. K.; Ray, A.; Mukhopadhyay, I. Electrodeposition of Si from an Ionic Liquid Bath at Room Temperature in the Presence of Water. *Langmuir* **2017**, *33*, 1599−1604.
(56) Myung, N.; Rho, K.; Shon, E. B.; Park, T. W.; Kim, S. Y.; Kato, M.; Rajeshwar, K. Metal-Organic Frameworks as Synthetic Precursors for SILAR: A Tale of Two Oxides. *ECS J. Solid State Sci. Technol.* **2022**, *11*, 093007.
(57) Zhang, Z.; Wen, G.; Luo, D.; Ren, B.; Zhu, Y.; Gao, R.; Dou, H.; Sun, G.; Feng, M.; Bai, Z.; Yu, A.; Chen, Z. Two Ships in a Bottle" Design for Zn-Ag-O Catalyst Enabling Selective and Long-Lasting CO_2 Electroreduction. *J. Am. Chem. Soc.* **2021**, *143*, 6855−6864.
(58) O'Donnell, S.; Vali, A.; Rawat, A.; Maggard, P. A.; Huda, M. N.; Rajeshwar, K. Perspective—Multinary Oxide Semiconductors for Solar Fuels Generation: Closing the Performance Gap between Theory and Practice. *ECS J. Solid State Sci. Technol.* **2022**, *11*, 053001.

https://doi.org/10.1021/acs.accounts.2c00838
Acc. Chem. Res. 2023, 56, 994−1003